TiO₂, surface modified TiO₂ and graphene oxide-TiO₂ photocatalysts for degradation of water pollutants under near-UV/Vis and visible light

Luisa M. Pastrana-Martínez[a], Sergio Morales-Torres[a], Athanassios G. Kontos[c], Nikolaos G. Moustakas[c], Joaquim L. Faria[a], José M. Doña-Rodríguez[b,*], Polycarpos Falaras[c,*], Adrián M.T. Silva[a,*]

a LCM – Laboratory of Catalysis and Materials – Associate Laboratory LSRE/LCM, Faculdade de Engenharia, Universidade do Porto, Rua Dr. Roberto Frias, 4200-465 Porto, Portugal. Fax: +351-22-5081449; Tel: +351-22-5081582

bFEAM-Departamento de Química. Universidad de Las Palmas de Gran Canaria Edificio Central del Parque Científico-Tecnológico de la ULPGC. Campus Universitario de Tafira, 35017-Las Palmas, Spain.

c Institute of Advanced Materials, Physicochemical Processes, Nanotechnology and Microsystems (IAMPPNM), Division of Physical Chemistry, NCSR Demokritos, 15310 Aghia Paraskevi, Attikis, Athens, Greece. Fax: +30-210-6511766; Tel: +30-210-6503644

*Corresponding authors e-mail addresses:

adrian@fe.up.pt (A.M.T. Silva); papi@chem.demokritos.gr (P. Falaras); jdona@dqui.ulpgc.es (J.M. Doña-Rodríguez).

26   **Abstract**

27   In this work the photocatalytic activity between a TiO_2 catalyst synthetized by a modified sol-

28   gel method (ECT), TiO_2 nanoparticles surface modified with organic shell layer (m-TiO_2) and a

29   graphene oxide-TiO_2 composite (GOT-3.3) was compared. Diphenhydramine (DP)

30   pharmaceutical and methyl orange (MO) azo-dye were used as model water pollutants under

31   both near-UV/Vis and visible light irradiation. The TiO_2 photocatalyst from Evonik Degussa

32   Corporation (P25) was used as reference material and the pseudo-first order rate constants (k)

33   and total organic carbon (TOC) removal were determined.

34   Under near-UV/Vis irradiation, the results show that ECT and GOT-3.3 are highly active

35   photocatalysts for the degradation of DP ($k = 64.5 \times 10^{-3}$ and 62×10^{-3} min^{-1}, respectively) and

36   mineralization (TOC removal of 55% and 50%, respectively) being the overall performance

37   comparable to that obtained with P25 ($k = 56 \times 10^{-3}$ min^{-1} and 48% of TOC removal). The

38   composite GOT-3.3 presents a markedly higher activity for conversion of the MO dye ($k =$

39   126×10^{-3}, 52×10^{-3}, 49×10^{-3}, 18.1×10^{-3} min^{-1} for GOT-3.3, P25, ECT and m-TiO_2, respectively)

40   as well as for its mineralization, with TOC removals tailoring the same order. Under visible light

41   illumination, P25 is practically inactive and GOT-3.3 (for DP) and m-TiO_2 (for MO) are the

42   photocatalysts with better properties than P25, or even than ECT.

43   Scavenger agents were used as a diagnostic tool for the analysis of the photocatalytic

44   mechanism, being defined three ratios to understand the relevance of each step in this

45   mechanism. Regarding DP, it was concluded that direct oxidation by photogenerated holes is

46   more important for the modified TiO_2 materials (m-TiO_2 and GOT-3.3) than for ECT and P25

47   which present higher availability to generate radical species from photoinduced holes. A

48   photoreduction mechanism on the surface of the photocatalysts was observed for MO, the

49   addition of EDTA (electron donor) greatly enhancing the rate of MO photoreduction.

1. Introduction

Heterogeneous photocatalysis is one of the most promising advanced oxidation processes with wide applications in environmental remediation and solar energy conversion. Different strategies have been employed to enhance the efficiency of the photocatalytic materials, aiming lower recombination rate for the produced electron–hole pairs and narrowed band gap energy, in particular for titania (TiO$_2$) which is the most common photocatalyst.

In this line, the typical methods of synthesis (e.g., sol-gel, hydrothermal, solvothermal) have been optimized with the objective to tailor the TiO$_2$ crystalline phase and particles size [1, 2]. Various approaches have been used in the literature [3] in order to extend the TiO$_2$ photorespond in the visible and allow solar driven photocatalytic applications. Among the most promising, anion doping of TiO$_2$ [4, 5] and co-sensitization of TiO$_2$ with inorganic or organic compounds [6] are mentioned. Alternatively TiO$_2$ can be combined with nanostructured carbon materials, either in core shell structures or by using single- and multi-walled carbon nanotubes [7, 8], fullerenes [9, 10] and graphene [11, 12] . Among those graphene is recently emerging as one of the most promising to produce next generation photocatalysts [13], with excellent mobility of charge carriers, large specific surface area, flexible structure, high transparency and good electrical and thermal conduction [14].

In the present work the effectiveness of three photocatalysts (prepared by three different approaches in the frame of the Clean Water European project – GA n°227017), and used for the degradation and mineralization of two hazardous pollutants - diphenhydramine (DP) pharmaceutical and methyl orange (MO) azo dye - under both near-UV/Vis and visible light irradiation, is compared for the first time. These photocatalysts were used at the previously optimized conditions of synthesis, namely: (i) a TiO$_2$ photocatalyst (ECT) prepared by a

3

modified sol-gel method [1]; (ii) a surface modified nanoparticulate titania (m-TiO$_2$) photocatalyst with visible light activity [15]; and (iii) a graphene oxide-TiO$_2$ composite (GOT-3.3) synthetized by liquid phase deposition [16]. The possible pathways for photocatalytic degradation were examined through the use of scavengers for both radicals and holes (*t*-BuOH and EDTA, respectively), and three different ratios were defined to illustrate the significance of each step in the photodegradation mechanism, namely: *(1)* oxidation by reactive radicals formed from photoexcited electrons; *(2)* direct oxidation by photogenerated holes; and *(3)* oxidation by reactive radicals formed from photoinduced holes.

2. Experimental

2.1. Reagents and materials

High-purity analytical grade diphenhydramine (DP, 99%), methyl orange (MO, 99%) and *tert*-butanol (*t*-BuOH, $\geq$ 99.7%) were obtained from Sigma-Aldrich and ethylenediaminetetraacetic acid (EDTA, > 99%) from Fisher Scientific. Acetonitrile ($\geq$ 99.8%) was used with HPLC grade (Chromanorm). Ammonium hexafluorotitanate (> 99.99%), boric acid (> 99%), titanium butoxide (97.0%) and tetrabutyl titanate (97.0%) were obtained from Sigma-Aldrich. Ethanol (99.5%), citric acid (99.5%) and urea (25% w/v) were supplied by Panreac.

2.2. Catalysts synthesis and characterization

ECT-1023t (referred in the present work as ECT) was synthesized following a sol-gel procedure (using titanium butoxide as precursor) and a calcination temperature of 750 ºC which allows tailoring the optimal size, crystallinity and surface area of TiO$_2$ particles. Modified TiO$_2$ (m-TiO$_2$) nanoparticles, that already proved enhanced photocatalytic activity under visible light irradiation [15], were synthesized by hydrolysis condensation of tetrabutyl titanate following combustion with urea, at a calcination temperature of 450 ºC. GOT-3.3-200 (referred in the

present work as GOT-3.3) was prepared by liquid phase deposition (using ammonium

hexafluorotitanate as precursor) with an optimal graphene oxide content of 3.3 wt.% and 200 ºC

as temperature of treatment. These three materials were fully characterized elsewhere [1, 15,

16], some of the most characteristic information is shown in Table 1. The TiO_2 photocatalyst

from Evonik Degussa Corporation (P25) was used as reference material.

2.3. Photocatalytic experiments

The photocatalytic degradation of DP (3.40×10^{-4} mol L^{-1}) or MO (3.05×10^{-5} mol L^{-1}) was

carried out at room temperature (25 ºC) in aqueous solutions under near-UV/Vis and visible

light irradiation. The experiments were performed in a quartz cylindrical reactor filled with 7.5

mL of the selected model pollutant, as described elsewhere [16]. Briefly, a Heraeus TQ 150

medium-pressure mercury vapour lamp was used as irradiation source delivering near-UV/Vis

irradiation ($\lambda > 350$ nm; 50 mW cm^{-2}) and for visible light experiments a cut-off long pass filter

was used ($\lambda > 430$ nm; 6 mW cm^{-2}). Before turning on the lamp, the suspensions were saturated

with an oxygen flow and magnetically stirred for 30 min to establish an adsorption-desorption

equilibrium. The optimal catalyst load was established in preliminary photocatalytic

experiments with the aim to avoid the ineffective excess of catalyst (1.0 g L^{-1} and 0.5 g L^{-1} for

DP and MO, respectively). Experiments in the absence of catalyst were also performed to

determine the contribution from direct photolysis. The optimal operating pH values used for the

photocatalytic runs (4.4 for MO and natural pH of 5.9 for DP) were selected in preliminary

experiments performed at different pH values, both pollutants being present in their protonated

form at such conditions.

The concentration of DP was measured by HPLC with a Hitachi Elite LaChrom system

equipped with a Hydrosphere C18 column. The concentration of MO was determined by UV-

Vis spectrophotometry at the characteristic wavelength reported in literature of 464 nm [3], by

using a Jasco V-560 spectrophotometer. The total organic carbon (TOC) was also determined

127 for selected samples using a Shimadzu TOC-5000A analyzer. Trapping experiments of holes

128 and radicals were performed by adding excess of EDTA or *t*-BuOH, respectively.

129 The photocatalytic oxidation of the tested pollutants can be ascribed to a pseudo-first order

130 kinetic model, as described by the following equation:

131 $\qquad C = C_0\,e^{-kt}$ (1)

132 where C corresponds to pollutant concentration, k is the pseudo-first order kinetic constant, t is

133 the reaction time and C_0 is the pollutant concentration for $t = 0$. The values of k were obtained

134 by non-linear regression. Table 2 shows the k constants (with respective standard errors)

135 obtained by fitting the model described in Eq. (1), the coefficient of variation, CV, expressed in

136 percentage as k_{CV} (standard error×100/parameter value) and the respective regression coefficient

137 (r^2), in general indicating a good fitting of the model to the experimental data.

138

139 **3. Results and discussion**

140 *3.1. Catalyst characterization*

141 Table 1 contains the BET surface area (S_{BET}), relative amount of anatase and rutile crystalline

142 phases and corresponding crystallites size, as well as the band-gap energy (E_g) of the different

143 catalysts. The TiO_2 nanoparticles prepared by sol gel method (ECT) present the lowest BET

144 surface area (18 $m^2\,g^{-1}$) and the highest anatase average particle size (57 nm), with some rutile

145 crystalline phase (6-11%). These characteristics have been attributed to the acid used in the

146 synthesis (citric acid), the removal of the largest aggregates before the calcination step (by

147 sieving) and respective calcination temperature (750 ºC) employed during the synthesis of this

148 material [1]. m-TiO_2 and GOT-3.3 present larger surface area ($S_{BET} = 141$ and 117 $m^2\,g^{-1}$,

149 respectively) and exclusively anatase TiO_2 particles with an average anatase particle size of 8

150 and 4 nm, respectively [15, 16].

151 All the photocatalysts present a narrowed band-gap than P25 ($E_g = 2.97$, 2.95, 2.28 and 3.18 eV

152 for ECT, GOT-3.3, m-TiO_2 and P25, respectively). In the case of ECT, the obtained band-gap

was mainly attributed to the particle size and crystallinity of this material [1] and for GOT-3.3

composite the band-gap narrowing was attributed to the chemical bonding between TiO_2 and the

specific sites of carbon (Ti-O-C bond) [16], as already observed for other carbonaceous

materials combined with TiO_2 [17]. The surface modified photocatalyst has the highest shift of

the energy band gap to the visible range (E_g = 2.28 eV) due to its sensitization with visible light

active carbonaceous species and forms a well defined inorganic/organic heterojunction,

suggesting at this point that the m-TiO_2 catalyst could be the most efficient photocatalyst, at

least under visible light illumination [15].

3.2. DP photocatalytic degradation

The photocatalytic activity of the prepared catalysts as well as that of the benchmark P25

material was evaluated in the photodegradation of DP under near-UV/Vis (Fig. 1a) and visible

light (Fig. 1b) illumination. The kinetic parameters of the time profiles are gathered in Table 2.

3.2.1. Near-UV/Vis irradiation

The direct photolysis of DP aqueous solutions was first investigated in order to quantify the

amount of DP degraded under non-catalytic conditions, being observed that such a contribution

is practically negligible. Thus, DP is very resistant to photodegradation under near-UV/Vis light

irradiation in the absence of a catalyst ($k = 1.0 \times 10^{-3}$ min^{-1}).

The photocatalytic efficiency of the tested materials for DP degradation under near-UV/Vis

irradiation is shown in Fig. 1a and Table 2. The results indicate that GOT-3.3, ECT and P25 are

very active photocatalysts, with comparable efficiency, for DP degradation (k = 64.5×10^{-3},

62×10^{-3} min^{-1} and 56×10^{-3} min^{-1} for ECT, GOT-3.3 and P25, respectively). The lowest DP

photocatalytic degradation in such conditions (9.6×10^{-3} min^{-1}) was obtained for the m-TiO_2

catalyst. The same tendency was observed for the DP mineralization; i.e., after 60 min of near-

UV/Vis irradiation; ECT, GOT-3.3 and P25 photocatalysts produced a TOC reduction of 53%, 50% and 48%, respectively, while m-TiO$_2$ leads to a TOC reduction of only 23% (Fig. 2a).

In our previous studies using ECT as catalyst and different model pollutants (including phenol, formic acid, dichlorophenoxyacetic acid and MO) [1, 18], the high efficiency of ECT has been always attributed to the enhanced formation of reactive hydroxyl radicals at the catalyst surface. The efficiency of ECT for the particular degradation of DP as model water model pollutant has been recently evaluated [19], taking into account different operating parameters such as catalyst loading and initial solution pH; and these results also confirmed that the high efficiency of ECT is mainly attributed to formation of the reactive hydroxyl radicals at the catalyst surface.

In another work [16], the effects of the graphene oxide content and the respective treatment temperature have been systematically investigated on the photocatalytic efficiency of GOT composites under near-UV/Vis and visible light irradiation for degradation of DP and MO. The efficiency of the most active composite (there referred as GOT-3.3-200 and corresponding in the present work to GOT-3.3) was in this case attributed to the optimal assembly and interfacial coupling between the graphene oxide sheets and TiO$_2$ nanoparticles, allowing graphene oxide to generate more reactive radicals than the respective bare TiO$_2$ material via the reaction of stored and transported electrons from near-UV/Vis irradiated TiO$_2$.

3.2.2. Visible light illumination

Regarding visible light illumination, Fig. 1b show the results obtained for DP degradation with all materials tested and under the same reaction time used for near-UV/Vis light irradiation (i.e. 60 min). The inset of Fig. 1b shows the data for a longer reaction time (240 min) with the aim to better compare the efficiency between the tested catalysts, the respective pseudo-first order rate constants being shown in Table 2. As expected, the pseudo-first order rate constants under visible light illumination are lower than those obtained under near-UV/Vis irradiation because the same lamp was used in both cases and the cut-off long pass filter (used in visible light experiments) allows only photons with $\lambda > 430$ nm to the sample. In these conditions, GOT-3.3

and then m-TiO$_2$ have the highest photocatalytic activity for DP degradation under visible light illumination, better than the TiO$_2$ materials, i.e., ECT and P25 (k = 4.4×10^{-3}, 1.35×10^{-3}, 0.75×10^{-3} and 0.49×10^{-3} min^{-1} for all of them, respectively). In fact, the pseudo-first order rate constant of P25 was very similar to that obtained for photolysis (0.40×10^{-3} min^{-1}), indicating as expected that P25 is practically inactive for activation with photons of wavelength above 430 nm. Regarding the mineralization (Fig. 2a), the TOC reduction follows the same trend observed for DP degradation (i.e., GOT-3.3 > m-TiO$_2$ > ECT > P25).

Therefore, GOT-3.3, and ECT and P25 are efficient materials for photocatalytic reactions under near-UV/Vis irradiation, while GOT-3.3 and then m-TiO$_2$ are more appropriate for visible (λ > 430 nm) light applications. This is a clear indication that the activation mechanisms are different for each material, but GOT-3.3 is able to switch between the more appropriate pathway defining on excitation.

3.3. MO photocatalytic degradation

The photocatalytic activity of the different materials was also investigated for the degradation of MO under both near-UV/Vis and visible light. The kinetic parameters are gathered in Table 2.

3.3.1. Near-UV/Vis irradiation

The pseudo-first order rate constants for MO degradation under near-UV/Vis irradiation (Fig. 1c and Table 2) follow the sequence: GOT-3.3 (126×10^{-3} min^{-1}) >> P25 (52×10^{-3}) ~ ECT (49×10^{-3} min^{-1}) >> m-TiO$_2$ (18.1×10^{-3} min^{-1}), the GOT composite presenting a markedly higher photocatalytic activity for MO abatement than the other materials tested. A similar trend was found concerning the TOC reduction under near-UV/Vis irradiation (Fig. 2b): GOT-3.3 (45%) > P25 (37%) ~ ECT (35%) > m-TiO$_2$ (20%), indicating that GOT composites with optimal content of graphene oxide have extended photocatalytic activity under near-UV/Vis irradiation for

227 degradation of the MO azo dye in comparison with the other materials at the experimental

228 conditions tested.

229 In fact, composites based on graphene oxide and TiO_2 have already shown to be highly active

230 photocatalysts for different azo dyes, such as MO [11], rhodamine B [12, 20], and methylene

231 blue [21]. In particular it has been recently reported by our group [16] that composites with an

232 optimal graphene oxide content (3.3-4.0 wt.%) may effectively enhance the photocatalytic

233 activity of TiO_2 in the visible range without compromising the performance under UV

234 irradiation, a major drawback usually associated to visible light active anion doped TiO_2

235 photocatalysts. In fact, the P25 photocatalyst showed slightly better performance than ECT for

236 MO degradation under near-UV/Vis irradiation ($k = 52 \times 10^{-3}$ and 49×10^{-3}, respectively).

237 However, it is important to refer that ECT has proved to be more effective than P25 for several

238 organic pollutants, even MO, but in other conditions (including radiation source and catalyst

239 load) [1, 18].

240 *3.3.2. Visible light illumination*

241 The results obtained for MO degradation under visible light irradiation are presented in Fig. 1d

242 and Table 2. The corresponding pseudo-first order rate constants obtained with the experiments

243 performed in 240 min ($k = 10.0 \times 10^{-3}$, 7.5×10^{-3} and 1.1×10^{-3} min^{-1}, respectively for m-TiO_2,

244 GOT-3.3 and ECT) are higher than that obtained for P25 (0.58×10^{-3} min^{-1}) in the degradation of

245 MO (as observed for DP), indicating that all the methods of synthesis used lead to

246 photocatalysts with better properties than the benchmark catalyst for visible light applications. It

247 is also of interest to note that M-TiO_2 exhibited the highest photocatalytic activity for MO

248 degradation under visible light irradiation (in contrast with results obtained for DP) and that the

249 same tendency was observed in terms of TOC removal (Fig. 2b): m-TiO_2, GOT-3.3, ECT and

250 P25 produced respectively 22%, 18%, 4% and 3% of TOC reduction after 240 min of

251 irradiation. The high visible light photocatalytic activity of m-TiO_2 observed towards

252 degradation of MO (and also DP and microcystin-LR) may be justified by the red-shift of the

253   energy band gap to the visible range - about 2.28 eV. Furthermore, preliminary experiments in

254   the absence oxygen with m-TiO$_2$ (not shown) revealed that the photocatalytic activity of this

255   material strongly decreases at such conditions ($k = 10.0 \times 10^{-3}$ or 1.2×10^{-3} min^{-1} in the presence or

256   absence of oxygen, respectively), thus O$_2^{\bullet-}$ or even its product ^{1}O$_2$ could play an important role

257   in the photocatalytic degradation of MO under visible light.

258   Therefore, the results obtained with MO showed that at the tested conditions the composite

259   prepared with TiO$_2$ and graphene oxide (GOT-3.3) exhibited the highest activity under near-

260   UV/Vis irradiation while both modified TiO$_2$ (m-TiO$_2$) and GOT-3.3 presented the better

261   photocatalytic activity under visible light illumination.

262

263   *3.4. Pathway for photocatalytic degradation*

264   The pathways for photocatalytic degradation were investigated by isolating the main oxidative

265   routes of the photodegradation process. For this purpose, EDTA and *t*-BuOH were used as hole

266   and radical scavengers, respectively, to detect the prevalent oxidative pathways that participate

267   in the process, as indicated in literature [22, 23].

268   In Fig. 3a the pseudo-first order rate constants for the degradation of DP under near-UV/Vis

269   irradiation are shown with the scavengers for the prepared materials and also for P25. The

270   results show that the presence of *t*-BuOH as radical scavenger produced a decrease of the

271   pseudo-first order rate constants for all the catalysts tested, but the addition of EDTA reduced in

272   a much higher extent the DP photodegradation reaction rate (Table 2), e.g., in the respective

273   presence of *t*-BuOH or EDTA, from 64.5×10^{-3} min^{-1} to 18×10^{-3} or 2.1×10^{-3} min^{-1} for ECT and

274   from 62×10^{-3} min^{-1} to 29×10^{-3} or 6.8×10^{-3} min^{-1} for GOT-3.3. The decrease of the pseudo-first

275   order rate constant for DP corresponds to 97%, 92%, 89% and 79% with the addition of EDTA

276   and to 71%, 57%, 54% and 46% in the presence of *t*-BuOH for ECT, P25, GOT-3.3 and M-

277   TiO$_2$, respectively.

278 Therefore, it is clear that reactive species such as hydroxyl ($HO^{\bullet}$) and possible others ($O_2^{\bullet-}$ or

279 $HOO^{\bullet}$) radicals (or even $^1O_2$) participate in the photocatalytic mechanism under near-UV/Vis

280 irradiation, but the photogenerated holes play a major role on the mechanism. In order to better

281 understand the effect of the scavengers on the reaction system, three different ratios were

282 defined considering a simplification of the photodegradation mechanism, as illustrated in Fig.

283 3c, where each ratio $k_{(i)}$ represents a *step i* of the process (*i = 1, 2, 3*), namely:

- **$k_{(1)}$** *= k_{EDTA}/k* represents *step (1)* - oxidation by reactive radicals (such as $O_2^{\bullet-}$) formed from photoexcited electrons, because photogenerated holes (h^+) are not available (they are trapped by EDTA) being inhibited *steps (2)* and *(3)*;

- **$k_{(2)}$** *= $k_{t\text{-}BuOH}/k$* represents *step (2)* - direct oxidation by photogenerated holes, because reactive radicals are not available (they are trapped by *t*-BuOH) being inhibited *steps (1)* and *(3)*;

- **$k_{(3)}$** *= $(k - k_{EDTA} - k_{t\text{-}BuOH})/k$* represents *step (3)* - oxidation by reactive radicals (e.g., $HO^{\bullet}$) formed from photoinduced holes, i.e. considering that $k = k_{(1)} + k_{(2)} + k_{(3)}$ and, as consequence, the $k_{(3)}$ ratio is determined by the difference between the pseudo-first order rate constant obtained in the absence of any scavenger (*k*) and the respective ratios obtained with EDTA and *t*-BuOH, $k_{(1)}$ and $k_{(2)}$, respectively.

295 where k_{EDTA} and $k_{t\text{-}BuOH}$ are the pseudo-first order rate constants obtained in the presence of

296 EDTA (holes captured) and *t*-BuOH (radicals captured), respectively. Table 3 shows the $k_{(i)}$

297 ratios for the oxidation paths of DP, for all materials. Since the values obtained for $k_{(2)}$ and $k_{(3)}$,

298 related to photogenerated holes, are higher than those obtained for $k_{(1)}$, related to photoexcited

299 electrons, the mechanism mediated by holes (both direct oxidation - $k_{(2)}$ - and formation of

300 reactive radicals - $k_{(3)}$) is more important for all tested materials than the mechanism mediated

301 by photoexcited electrons - $k_{(1)}$.

In particular, for *steps (1)* and *(2)* the respective ratios ($k_{(1)}$ and $k_{(2)}$) decrease as follows: M-TiO$_2$ > GOT-3.3 > P25 > ECT in contrast with the order determined for *step (3)*, i.e. $k_{(3)}$: ECT > P25 > GOT-3.3 > M-TiO$_2$. Therefore, since the determined ratios give an indication of how important is a step for the different materials, these values suggest that direct oxidation by photogenerated holes - $k_{(2)}$ (and then in less extent oxidation by radicals formed from photoexcited electrons - $k_{(1)}$) are more important for the modified TiO$_2$ materials (M-TiO$_2$ and GOT-3.3) than for bare TiO$_2$ materials (P25 and ECT). Moreover, the results suggest that ECT is more succeeded than other materials to generate reactive radicals from photoinduced holes - $k_{(3)}$, confirming the already observed higher availability of ECT in comparison with P25 to generate such radicals [1, 19], and being validated in this work such catalytic property of ECT when compared with completely different materials (m-TiO$_2$ and GOT-3.3).

Under visible light illumination, GOT-3.3 shows significant photocatalytic activity for DP degradation (Fig. 1b and Table 2) and it has been already shown [16] that the presence of radicals and holes scavengers reduces the rates of photocatalytic oxidation, this reduction being equivalent for both scavengers.

The same methodology was applied for MO photocatalytic experiments under near-UV/Vis. Fig. 3b show that the addition of *t*-BuOH (radicals scavenger) leads to an expected decrease of the pseudo-first order rate constants; however, the presence of EDTA (electron donor) enhanced greatly the rate of MO photoreduction, respectively: (i) from 126×10^{-3} to 559×10^{-3} min^{-1} for GOT-3.3; (ii) from 49×10^{-3} to 309×10^{-3} min^{-1} for ECT; (iii) from 18.1×10^{-3} to 90×10^{-3} min^{-1} for M-TiO$_2$; (iv) from 52×10^{-3} to 536×10^{-3} min^{-1} for P25. These high values obtained for the pseudo-first order rate constants in the presence of EDTA are justified by the MO photoreduction mechanism on the surface of the photocatalyst that has been already reported for several photocatalysts when EDTA was used, including TiO$_2$/zeolite [24]. Other electron donors were also tested in this work (formic acid and ascorbic acid), but the same behaviour was observed, i.e. a MO photoreduction mechanism. In the particular case of EDTA, this electron

328 donor reacts with the strongly oxidizing photogenerated holes, inhibiting electrons-holes

329 recombination and by this way more excited electrons are available for reduction of MO to the

330 hydrazine derivative (the MO band detected at 464 nm disappearing during the reaction while a

331 new band assigned to the hydrazine derivative increases at 247 nm) while reducing radicals

332 produced from EDTA by *H* abstraction could also enhance MO reduction. Hydrazine has been

333 classified as human carcinogen by Environmental Protection Agency (EPA) and, in this context,

334 analysis of toxicity will be required in further experiments.
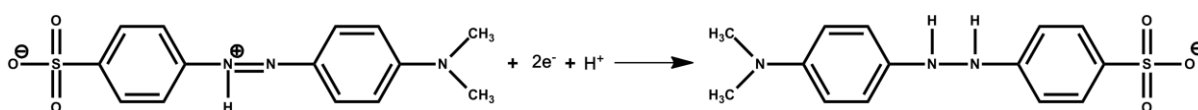
335
336 Therefore, the nitrogen–nitrogen double bond (–N=N–) responsible for the characteristic colour

337 of MO is broken up assuming that MO photoreduction occurs in the same way as it was

338 determined by Brown et al. [25]. Even so, the decrease of rate constants in presence of *t*-BuOH

339 and in particular the TOC reduction that was observed in the experiments with all catalysts

340 tested (Fig. 2b) confirmed the photocatalytic degradation and mineralization of MO at the tested

341 conditions.

342

343 **Conclusion**

344 Three different TiO_2 catalysts, large titania sol-gel nanoparticles (ECT), surface modified titania

345 nanoparticles (m-TiO_2) and graphene oxide-TiO_2 composite (GOT-3.3), were compared in terms

346 of their photocatalytic properties.

347 Under near-UV/Vis irradiation, ECT is one of the most active photocatalysts for the degradation

348 of DP. The higher efficiency of ECT is related to its enhanced availability to originate reactive

349 hydroxyl radicals from photoinduced holes at the catalyst surface.

350 GOT-3.3 composite is quite active in the photodegradation of both DP and MO pollutants,

351 especially under visible light, where P25 is practically inactive.

m-TiO$_2$ displayed a remarkable photocatalytic activity for degradation of MO under visible light irradiation, suggesting promising results for visible light applications.

For all catalysts tested for the photocatalysis of DP, the photogenerated holes are the main reactive species (in comparison to the radicals formed from photoexcited electrons). In particular, direct oxidation by photogenerated holes play a major role in the case of m-TiO$_2$ and GOT-3.3, when compared with bare TiO$_2$ materials (ECT and P25). In the case of MO, a photoreduction mechanism on the TiO$_2$ surface was observed, involving the photoinduced electrons. This is confirmed by the significant enhancement of the photocatalytic rate upon addition of EDTA holes scavengers that results in the inhibition of electron-hole recombination.

References

[1] J. Araña, J.M. Doña-Rodríguez, D. Portillo-Carrizo, C. Fernández-Rodríguez, J. Pérez-Peña, O. González Díaz, J.A. Navío, M. Macías, Photocatalytic degradation of phenolic compounds with new TiO$_2$ catalysts, Appl. Catal., B, 100 (2010) 346-354.

[2] M. Toyoda, Y. Nanbu, Y. Nakazawa, M. Hirano, M. Inagaki, Effect of crystallinity of anatase on photoactivity for methylene blue decomposition in water, Appl. Catal., B, 49 (2004) 227-232.

377 [3] M. Pelaez, N.T. Nolan, S.C. Pillai, M.K. Seery, P. Falaras, A.G. Kontos, P.S.M. Dunlop,

378 J.W.J. Hamilton, J.A. Byrne, K. O'Shea, M.H. Entezari, D.D. Dionysiou, A review on the

379 visible light active titanium dioxide photocatalysts for environmental applications, Appl. Catal.,

380 B, 125 (2012) 331-349.

381 [4] X. Zhou, F. Peng, H. Wang, H. Yu, J. Yang, Preparation of nitrogen doped TiO_2

382 photocatalyst by oxidation of titanium nitride with H_2O_2, Mater. Res. Bull., 46 (2011) 840-844.

383 [5] F. Dong, S. Guo, H. Wang, X. Li, Z. Wu, Enhancement of the Visible Light Photocatalytic

384 Activity of C-Doped TiO_2 Nanomaterials Prepared by a Green Synthetic Approach, J. Phys.

385 Chem. C, 115 (2011) 13285-13292.

386 [6] S.G. Kumar, L.G. Devi, Review on Modified TiO2 Photocatalysis under UV/Visible Light:

387 Selected Results and Related Mechanisms on Interfacial Charge Carrier Transfer Dynamics, J.

388 Phys. Chem. A, 115 (2011) 13211-13241.

389 [7] Y. Li, L. Li, C. Li, W. Chen, M. Zeng, Carbon nanotube/titania composites prepared by a

390 micro-emulsion method exhibiting improved photocatalytic activity, Appl. Catal., A, 427–428

391 (2012) 1-7.

392 [8] W. Wang, P. Serp, P. Kalck, J.L. Faria, Visible light photodegradation of phenol on MWNT-

393 TiO_2 composite catalysts prepared by a modified sol-gel method, J. Mol. Catal. A-Chem., 235

394 (2005) 194-199.

395 [9] S. Mu, Y. Long, S.-Z. Kang, J. Mu, Surface modification of TiO_2 nanoparticles with a C_{60}

396 derivative and enhanced photocatalytic activity for the reduction of aqueous Cr(VI) ions, Catal.

397 Commun., 11 (2010) 741-744.

398 [10] J. Yu, T. Ma, G. Liu, B. Cheng, Enhanced photocatalytic activity of bimodal mesoporous

399 titania powders by C_{60} modification, Dalton Trans., 40 (2011) 6635-6644.

400 [11] Z. Peining, A.S. Nair, P. Shengjie, Y. Shengyuan, S. Ramakrishna, Facile Fabrication of

401 TiO_2–Graphene Composite with Enhanced Photovoltaic and Photocatalytic Properties by

402 Electrospinning, ACS Appl. Mater. Interfaces, 4 (2012) 581-585.

403   [12] T.-D. Nguyen-Phan, V.H. Pham, H. Kweon, J.S. Chung, E.J. Kim, S.H. Hur, E.W. Shin,

404   Uniform distribution of TiO_2 nanocrystals on reduced graphene oxide sheets by the chelating

405   ligands, J. Colloid Interface Sci., 367 (2012) 139-147.

406   [13] S. Morales-Torres, L.M. Pastrana-Martínez, J.L. Figueiredo, J.L. Faria, A.M.T. Silva,

407   Design of graphene-based TiO_2 photocatalysts - A review, Environ. Sci. Pollut. Res., 19 (2012)

408   3676-3687.

409   [14] A.K. Geim, K.S. Novoselov, The rise of graphene, Nat. Mater., 6 (2007) 183-191.

410   [15] N.G. Moustakas, A.G. Kontos, V. Likodimos, F. Katsaros, N. Boukos, D. Tsoutsou, A.

411   Dimoulas, G.E. Romanos, D. D. Dionysiou, P. Falaras, Inorganic-organic core-shell titania

412   nanoparticles for efficient visible light activated photocatalysis, Appl. Catal., B, (2012) doi:

413   10.1016/j.apcatb.2012.1010.1007.

414   [16] L.M. Pastrana-Martínez, S. Morales-Torres, V. Likodimos, J.L. Figueiredo, J.L. Faria, P.

415   Falaras, A.M.T. Silva, Advanced nanostructured photocatalysts based on reduced graphene

416   oxide-TiO_2 composites for degradation of diphenhydramine pharmaceutical and methyl orange

417   dye, Appl. Catal., B, 123-124 (2012) 241-256.

418   [17] C.G. Silva, J.L. Faria, Photocatalytic oxidation of benzene derivatives in aqueous

419   suspensions: Synergic effect induced by the introduction of carbon nanotubes in a TiO_2 matrix,

420   Appl. Catal., B, 101 (2010) 81-89.

421   [18] C. Fernández-Rodríguez, J.M. Doña-Rodríguez, O. González-Díaz, I. Seck, D. Zerbani, D.

422   Portillo, J. Perez-Peña, Synthesis of highly photoactive TiO_2 and Pt/TiO_2 nanocatalysts for

423   substrate-specific photocatalytic applications, Appl. Catal., B, 125 (2012) 383-389.

424   [19] L.M. Pastrana-Martínez, J.L. Faria, J.M. Doña-Rodríguez, C. Fernández-Rodríguez,

425   A.M.T. Silva, Degradation of diphenhydramine pharmaceutical in aqueous solutions by using

426   two highly active TiO_2 photocatalysts: Operating parameters and photocatalytic mechanism,

427   Appl. Catal., B, 113–114 (2012) 221-227.

428 [20] F. Wang, K. Zhang, Reduced graphene oxide–TiO$_2$ nanocomposite with high

429 photocatalystic activity for the degradation of rhodamine B, J. Mol. Catal. A: Chem., 345 (2011)

430 101-107.

431 [21] Y. Zhang, Z.-R. Tang, X. Fu, Y.-J. Xu, Engineering the Unique 2D Mat of Graphene to

432 Achieve Graphene-TiO$_2$ Nanocomposite for Photocatalytic Selective Transformation: What

433 Advantage does Graphene Have over Its Forebear Carbon Nanotube?, ACS Nano, 5 (2011)

434 7426-7435.

435 [22] N. Serpone, I. Texier, A.V. Emeline, P. Pichat, H. Hidaka, J. Zhao, Post-irradiation effect

436 and reductive dechlorination of chlorophenols at oxygen-free TiO$_2$/water interfaces in the

437 presence of prominent hole scavengers, J. Photochem. Photobiol., A, 136 (2000) 145-155.

438 [23] C. Minero, G. Mariella, V. Maurino, D. Vione, E. Pelizzetti, Photocatalytic Transformation

439 of Organic Compounds in the Presence of Inorganic Ions. 2. Competitive Reactions of Phenol

440 and Alcohols on a Titanium Dioxide−Fluoride System, Langmuir, 16 (2000) 8964-8972.

441 [24] N. Dubey, S.S. Rayalu, N.K. Labhsetwar, R.R. Naidu, R.V. Chatti, S. Devotta,

442 Photocatalytic properties of zeolite-based materials for the photoreduction of methyl orange,

443 Appl. Catal., A, 303 (2006) 152-157.

444 [25] G.T. Brown, J.R. Darwent, Photoreduction of methyl orange sensitized by colloidal

445 titanium dioxide, J. Chem. Soc., Faraday Trans. 1, 80 (1984) 1631-1643.

446

447

448

449

450

451

452

453

454   **TABLES**

455

456

457   **Table 1.** Characterization of catalysts.

Catalyst	S_{BET} /(m^{2}g^{-1})	Crystalline phase (%)*	Particle size (nm)*	E_g (eV)
P25	52	80 (A) / 20 (R)	22 (A) / 25 (R)	3.18
ECT	18	89-94 (A) / 11-6 (R)	57 (A) / 86 (R)	2.97
m-TiO$_2$	141	100 (A)	8 (A)	2.28
GOT-3.3	117	100 (A)	4 (A)	2.95

458   * A: anatase; R: rutile.

459

460

461

462

463

464

465

466

467

468

469

470

471

472

473

474

Table 2. Pseudo-first order kinetic rate constant (k) of DP and MO degradation for different experimental conditions and respective coefficient of variation (CV), expressed as a percentage (k_{CV}) and regression coefficient (r^2).

	Diphenhydramine (DP)			Methyl orange (MO)		
	k (10^{-3} min^{-1})	k_{CV} (%)	r^2	k (10^{-3} min^{-1})	k_{CV} (%)	r^2
	near-UV/Vis (60 min)			near-UV/Vis (30 min)		
ECT	64.5 ± 0.6	1.0	0.9999	49 ± 5	8.8	0.99
ECT-EDTA	2.1 ± 0.1	7.4	0.98	309 ± 15	4.8	0.999
ECT- tBuOH	18 ± 1	5.3	0.99	23 ± 3	11.7	0.97
GOT-3.3	62 ± 3	4.2	0.998	126 ± 9	7.1	0.99
GOT-3.3-EDTA	6.8 ± 0.5	7.7	0.98	559 ± 5	9.6	0.998
GOT-3.3-tBuOH	29 ± 2	5.5	0.99	99 ± 7	6.8	0.99
m-TiO$_2$	9.6 ± 0.7	7.4	0.99	18.1 ± 0.6	3.5	0.997
m-TiO$_2$- EDTA	2.0 ± 0.1	5.3	0.99	90 ± 3	3.1	0.998
m-TiO$_2$- tBuOH	5.21 ± 0.04	0.8	0.9997	5.5 ± 0.6	10.1	0.97
P25	56 ± 4	6.7	0.998	52 ± 5	8.2	0.99
P25- EDTA	4.7 ± 0.9	18.4	0.9	536 ± 1	12.6	0.998
P25- tBuOH	24.3 ± 0.6	2.7	0.999	44 ± 4	9.4	0.99
Photolysis	1.00 ± 0.07	6.9	0.9	1.00 ± 0.20	9.6	0.9
	Visible (240 min)					
ECT	0.75 ± 0.07	9.1	0.97	1.1 ± 0.3	11.8	0.9
GOT-3.3	4.4 ± 0.1	2.9	0.999	7.5 ± 0.2	3.2	0.998
m-TiO$_2$	1.35 ± 0.06	4.5	0.99	10.0 ± 0.9	9.4	0.99
P25	0.49 ± 0.06	11.6	0.95	0.58 ± 0.08	13.0	0.92
Photolysis	0.40 ± 0.07	18.1	0.98	0.39 ± 0.05	11.4	0.94

Table 3. Ratios defined according to the contribution of each step of the simplified photodegradation mechanism of DP: *(1)* oxidation by reactive radicals formed from photoexcited electrons - $k_{(1)}$; *(2)* direct oxidation by photogenerated holes - $k_{(2)}$; and *(3)* oxidation by reactive radicals formed from photoinduced holes - $k_{(3)}$.

	$k_{(1)}$	$k_{(2)}$	$k_{(3)}$
ECT	0.033	0.28	0.69
GOT-3.3	0.11	0.47	0.42
m-TiO$_2$	0.21	0.54	0.25
P25	0.084	0.43	0.48

FIGURE CAPTION

509

510 **Figure 1.** Photocatalytic degradation over P25, ECT, m-TiO$_2$ and GOT-3.3 for (a-b) DP and (c-

511 d) MO under both near-UV/Vis and visible light irradiation. Curves represent the fitting of the

512 pseudo-first order equation to the experimental data (insets of (b) and (c) refer to data obtained

513 within 240 min).

514

515 **Figure 2.** Total organic carbon (TOC) reduction for the prepared catalysts and P25 under near-

516 UV/Vis and visible light irradiation for (a) DP and (b) MO.

517

518 **Figure 3.** Effect of EDTA and *t*-BuOH on the photocatalytic degradation under near-UV/Vis

519 irradiation for (a) DP and (b) MO and (c) main steps involved on the photocatalytic mechanism

520 and effect of scavengers for holes (EDTA) and radicals (*t*-BuOH).

521

522

523

524

525

526

527

528

529

530

531

532

533

534   **FIGURE 1**

535   **a)**
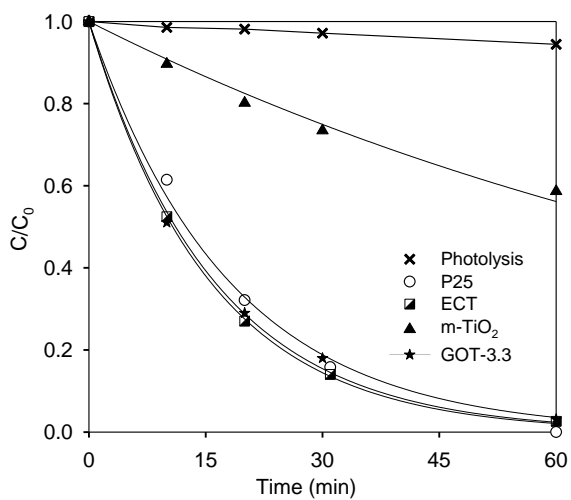
536

537   **c)**
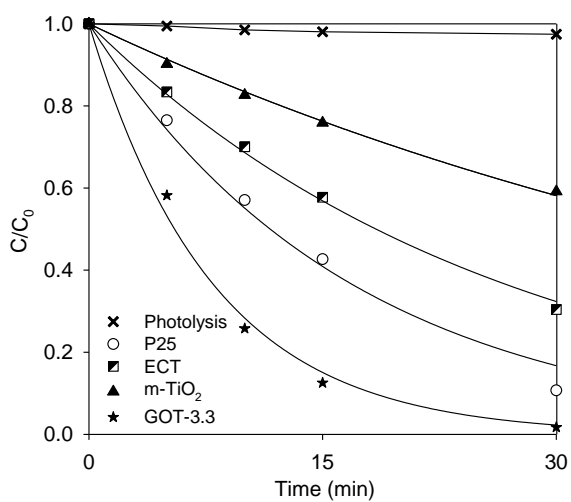
538
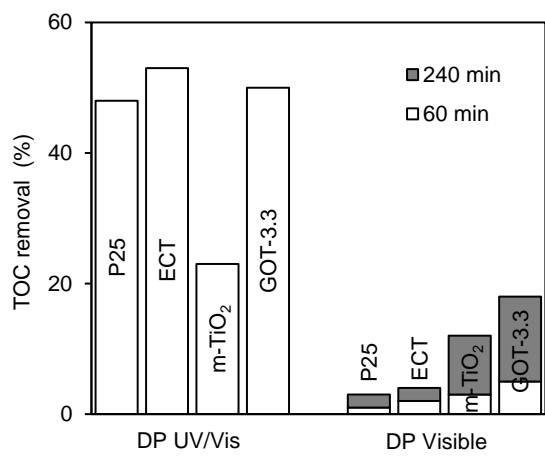
539

540

541

542

543

544

545

546
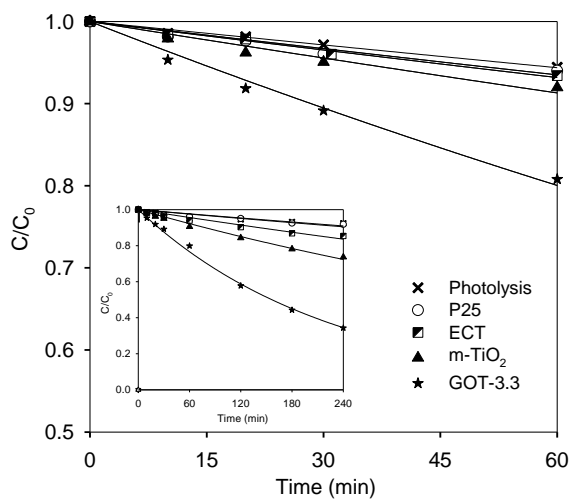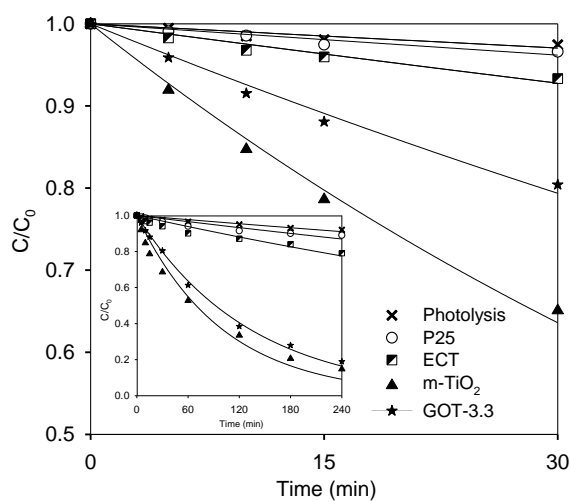
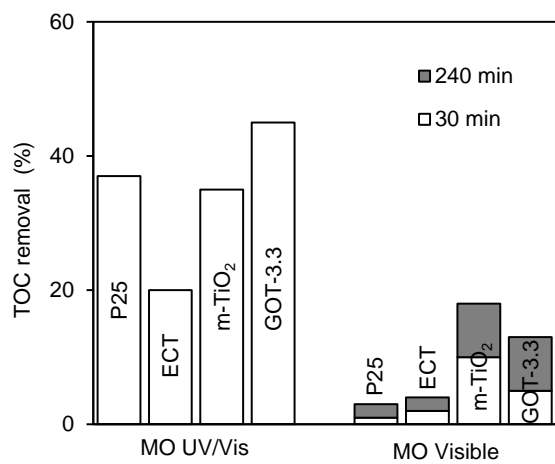547 **FIGURE 2**

548 **a)**

549

550

551 **b)**

552

553
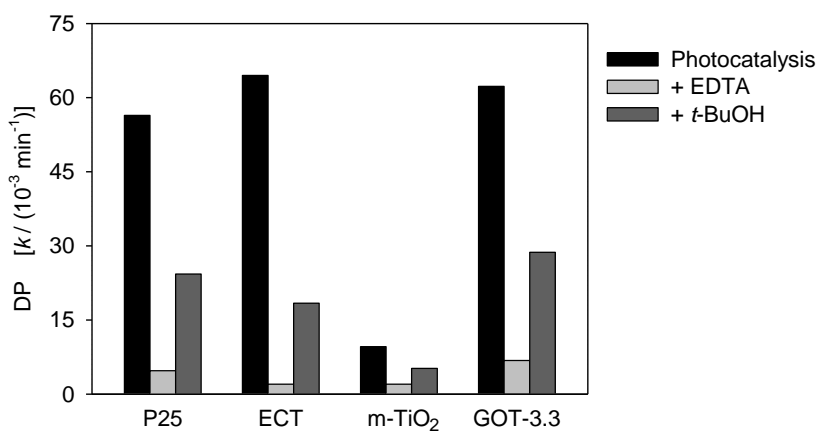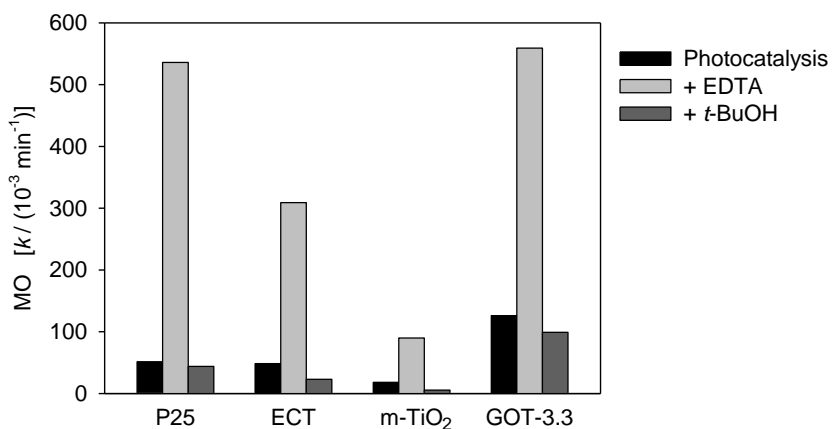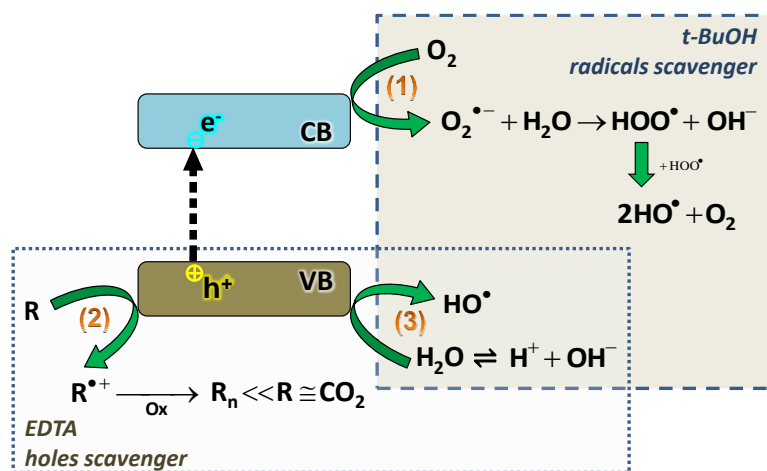
554

555

556

557

558

559

560

561 **FIGURE 3**

562 **a)**

563

564 **b)**

565

566 **c)**

567

568